A. Refractive index contrast measurements

The contrast factors, e.g. the change of the refractive index in dependence of temperature, T, and concentration, ω, are measured with an interferometer [1] and an Abbe refractometer (Anton Paar ABBEMAT RXA 158), respectively. For the calculation of S_T from the IR-TDFRS measurements, the contrast factors were interpolated from these measurement series for the correct temperatures and concentrations. $(\partial n/\partial T)_{p,\omega}$ is negative in the measured concentration and temperature range, the absolute value increases with higher formamide concentration and decreases with increasing temperature (Fig. S1).

Measurements of the refractive index were conducted for 11 concentrations ranging from pure water ($\omega = 0$) to pure formamide ($\omega = 1$) at 20, 35, 50 and 65°C. The measured values (Fig. S2) were fitted with a 2nd order polynomial and the slope of the resulting curves is $(\partial n/\partial \omega)_{p,T}$. The inset in Fig. S2 shows the behavior of the contrast factor: $(\partial n/\partial \omega)_{p,T}$ increases at higher formamide concentrations and decreases with rising temperature.
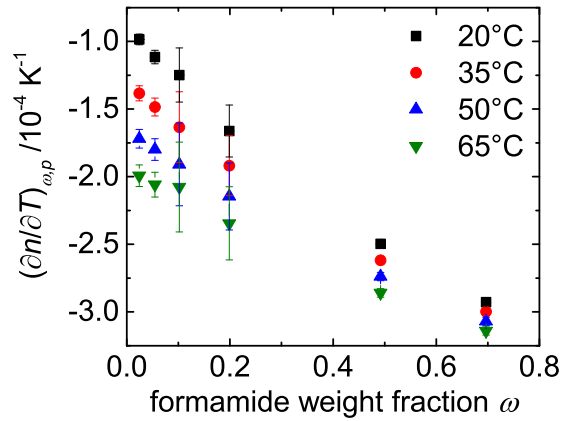

FIG. S1: Results of the interferometric measurement of the contrast factor $(\partial n/\partial T)_{p,\omega}$ as function of concentration, ω.
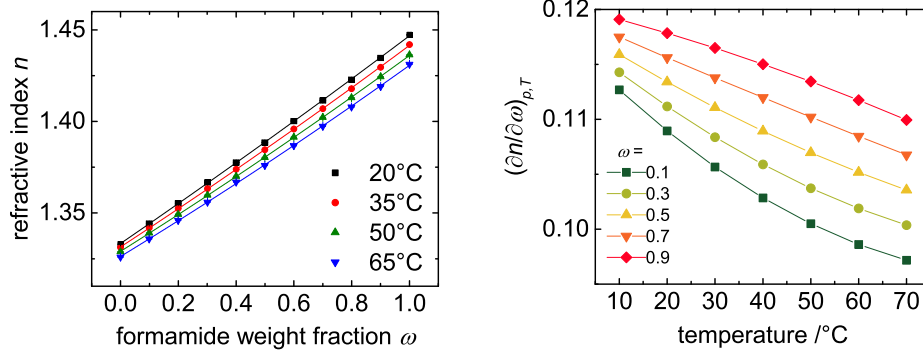
FIG. S2: (left) Concentration dependence of refractive index n at different temperatures. (right) Contrast factors $(\partial n/\partial \omega)_{p,T}$ determined from a polynomial fit as function of temperature.

B. Temperature and concentration dependence of the various quantities used as an input to the numerical calculations

The temperature and concentration dependence of the thermo- and mass diffusion ceofficient are obtained from IR-TDFRS measurements [2], which are shown in Fig. S3. For all investigated concentrations the mass diffusion coefficient shows only a slight decrease with increasing formamide concentration and increases significantly with rising temperatures, so that for the calculations we include only the temperature dependence and neglect the concentration dependence.
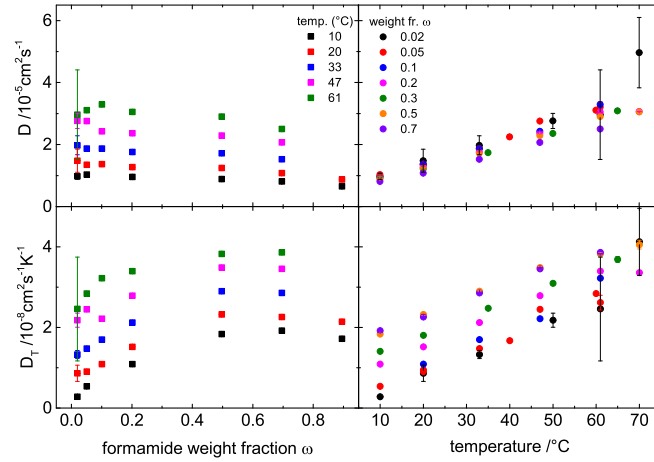

FIG. S3: Results of IR-TDFRS measurements. The mass diffusion coefficient D and thermal diffusion coefficient D_T as functions of the formamide weight fraction (left) and temperature (right).
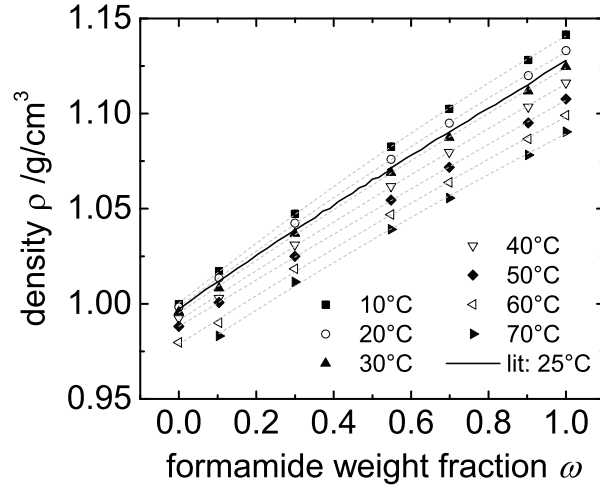
FIG. S4: Plot of the density values given in TABLE SI. The solid line represents literature values at 25°C [3].

From a fit to the diffusion coefficients, D, in Fig. S3 and of the Soret coefficients, S_T, in Fig.3 (main text) we obtain the following expressions, which are used for the calculations using the units given in Table SII,

$$D_T(T) = 3.36833 \cdot 10^{-5} \tag{1}$$
$$+(1.13331 \cdot 10^{-5} - 3.36833 \cdot 10^{-5})/(1 + (T/38.42736)^{4.08469}) \, ,$$

$$S_\text{T}(\omega, T) = (-2.55765 \cdot 10^{-4} + 2.34093 \cdot 10^{-5} \cdot T - 1.02968 \cdot 10^{-7} \cdot T^2) \tag{2}$$
$$+ \frac{\omega^{(0.6916 - 0.01459 \cdot T + 2.4822 \cdot 10^{-4} \cdot T^2)}}{(317.62149 + 1.03712 \cdot T + 0.18358 \cdot T^2) + \omega^{(0.6916 - 0.01459 \cdot T + 2.4822 \cdot 10^{-4} \cdot T^2)}} \, .$$

The specific mass density was measured over a range from 10 to 70°C for 5 mixtures with different weight fractions as well as pure water and formamide (see Table SI). Figure S4 compares the measured densities with the concentration dependent density at 25°C taken from literature [3], which agrees well with our data. From the experimental data, the following expression for the mass density is obtained,

$$\rho(\omega, T) = 1.00409 - 8.88391 \cdot 10^{-5} \cdot T - 4.97372 \cdot 10^{-6} \cdot T^2 \tag{3}$$
$$+ \left(0.03902 \cdot \exp\left(-\frac{T}{22.80603}\right) + 0.11532\right) \cdot \omega \, .$$

3

weight fraction ω	density ρ / g/cm^3						
	10°C	20°C	30°C	40°C	50°C	60°C	70°C
0.0000	0.99982	0.99832	0.99577	0.99236	0.98813	0.97965	-
0.1038	1.01727	1.01360	1.00824	1.00306	1.00065	0.99004	0.98309
0.2997	1.04737	1.04238	1.03694	1.03110	1.02490	1.01833	1.01142
0.5481	1.08271	1.07593	1.06900	1.06182	1.05446	1.046900	1.03916
0.6988	1.10244	1.09500	1.08740	1.07968	1.07181	1.06380	1.05563
0.9031	1.12822	1.12001	1.11178	1.10350	1.09514	1.08671	1.07825
1.0000	1.14151	1.13313	1.12465	1.11617	1.10765	1.09907	1.09044

TABLE SI: Density of formamide/water mixtures measured as a function of formamide weight fraction at temperatures from 10-70°C.

Experimental data for the shear viscosity, $\eta(\omega, T)$, of the mixture were taken from literature [4, 5],

$$\eta(\omega, T) = (0.03808 + 1.43946 \cdot 10^{-4} \cdot T) \cdot \exp\left(\frac{\omega}{0.20487 + 0.00189 \cdot T}\right) \tag{4}$$
$$+ (1.21076 - 0.01371 \cdot T) .$$

For the thermal conductivity, γ, the temperature dependence is negligible for both formamide [6] and water [7, 8]. The concentration dependence can be described by a linear function [9], and is accurately approximated by,

$$\gamma(\omega) = 0.5932 - 0.24653 \cdot \omega. \tag{5}$$

Experimental data for the specific heat capacity, C_P, of the formamide/water mixture are taken from Ref.[10], and are given by,

$$C_P(\omega, T) = 4168.383 + (-2441.1484 + 13.23161 \cdot T) \cdot \omega + 339.319 \cdot \omega^2 \tag{6}$$

The above expressions for the temperature and concentration dependencies are implemented in the COMSOL software for the calculation of the concentration- and flow profiles within the pores.

T	ω	ρ	η	γ	C_p	S_T	D
°C	weight fraction	g/cm^3	mPa$\cdot$s	W/(m$\cdot$K)	J/(kg$\cdot$K)	K^{-1}	cm^2/s

TABLE SII: Units used for the temperature, concentration, density, dynamic viscosity, thermal conductivity, specific heat capacity, Soret coefficient and mass diffusion coefficient in the specified expressions.
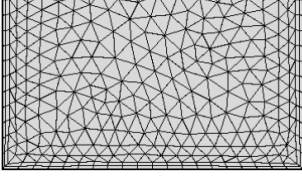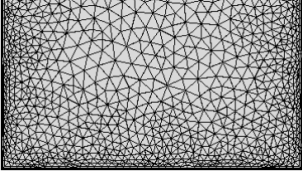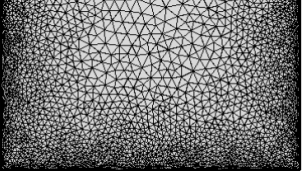
Mesh size	fine	finer	extra fine
Max. element size [m]	0.00117	8.14E-4	4.4E-4
Min. element size [m]	6.6E-6	2.75E-6	1.6E-6
Max. element growth rate	1.3	1.25	1.2
Curvature factor	0.3	0.25	0.25
Res. of narrow regions	1	1	1

TABLE SIII: Mesh sizes used for the simulations.

C. Numerical calculations

To calculate the accumulation of formamide in a hydrothermal pore we solved a combination of Navier-Stokes-, heat transfer-, and thermodiffusion equations using a commercially available finite element software (COMSOL Multiphysiscs 5.1). We carefully checked the consistency of the stationary and time dependent solutions, by varying the mesh size and length of the time steps (the mesh sizes that were used are shown in Table SIII). The *finer* and *extra fine* mesh gave identical results for the stationary states, while the *extra fine* mesh size was used for the time-dependent calculations in order to suppress an unphysical overshoot of the concentration for later times, just before the stationary state is reached.

The calculations were done for various aspect ratios of the pore at the optimal pore width. The optimal pore width depends on temperature. We used three different average temperatures for our calculations (25°C, 45°C and 75°C) and determined the optimal pore widths (180, 160 and 100 μm) for each temperature (see Fig.S5). With increasing temperature the optimal width decreases.

For the highest temperature, $T = 75°C$, we observe a strong decrease of the width, which might be related to the asymmetry of the velocity profile, which is discussed below.

Figure S6(left) shows the velocity profiles for the studied temperatures, Fig. S6(middle) the maximum velocity as function of the width and Fig. S6(right) the velocity versus the width of the pore. The latter contains information on the flow direction indicated by a sign change and illustrated by arrows in Fig. S6(left). Fig. S6(right) shows exemplary for one point how the maximum velocity is determined. The velocity profile in the pore is not dependent on width or height in the investigated range. At lower temperatures it is also independent of temperature. At very high temperatures the velocity profile shows an increased asymmetry with an up-flow stream that is much faster and narrower than the down-flow stream. The asymmetry is probably related to non-linear effects in the convective flow occurring for large temperature gradients and might also be responsible for the strong decrease of the optimal width at this high temperature. At $T = 75°C$ compared to the low temperatures the maximum velocity increases especially for the larger widths and leads to more mixing due to convection, therefore the width needs to be reduced to achieve large accumulation-folds.
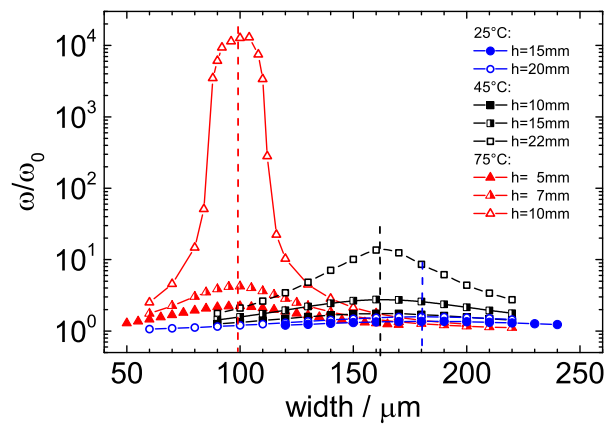

FIG. S5: The accumulation-fold, ω/ω_0, vs. width of the pore for T equal to 25°C (the blue symbols), 45°C (black) and 75°C (red). Dashed lines mark the optimal widths of 180, 160 and 100 μm at the respective temperatures of $T = 25, 45$ and 75°C.
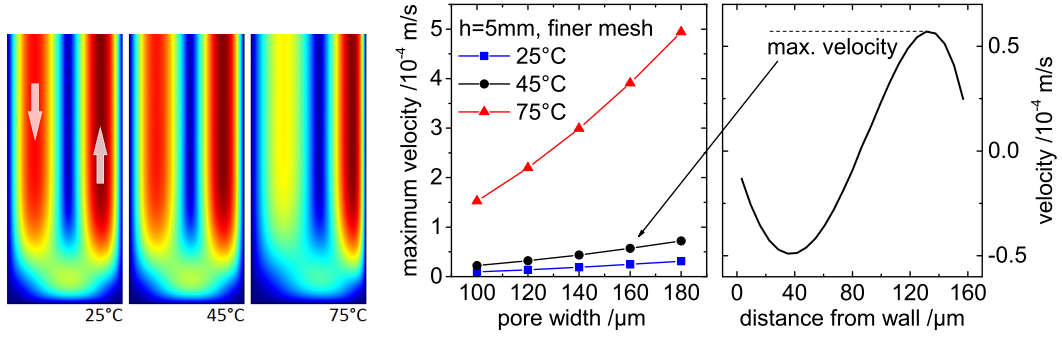
FIG. S6: (left) Relative velocity profiles at $T = 25$, 45 and 75°C. For each particular temperature dark blue and red refer to velocity=0 and highest velocity in the study, respectively. Note that the color code between different temperatures can not be compared. (middle) Maximum velocity vs. width at $T = 25, 45$ and 75°C. (right) Velocity profile in the pore with added information about flow direction.

Additonally we investigated how the accumulation-fold depends on the temperature difference, ΔT, across the pore. Figure S7(left) shows the accumulation-fold at $T = 75$°C as function of the aspect ratio for three different temperature differences across the pore. As expected a larger ΔT leads to a stronger accumulation, so that the plateau is reached at smaller aspect ratios.

Figure S7(right) shows the time dependence of the accumulation for different mean temperatures. It turns out that the time to reach the plateau, τ_{plateau} increases with increasing temperature. The physical reason for this behavior is that the convection process becomes stronger (Fig. S6) due to a decreasing viscosity with increasing temperature and leads to a stronger mixing so that a longer time is required to reach the plateau.
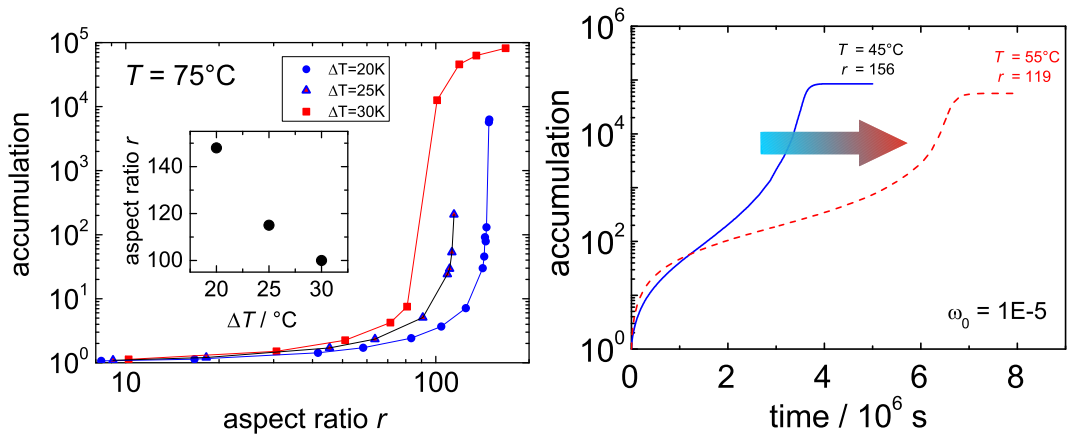
FIG. S7: (left)The accumulation-fold vs. aspect ratio at $T = 75°C$ for three different temperature differences ΔT. The inset shows the steep decrease of the aspect ratio, r, with increasing temperature difference, ΔT. (right) Accumulation as a function of time for two mean temperatures at an aspect ratio close to the plateau. The initial concentration was $\omega_0 = 1 \cdot 10^{-5}$.

[1] A. Becker, W. Köhler, and B. Müller, Ber. Bunsen-Ges. Phys. Chem. Chem. Phys. **99**, 600 (1995).

[2] S. Wiegand, H. Ning, and H. Kriegs, J. Phys. Chem. B **111**, 14169 (2007).

[3] E. P. Egan and B. B. Luff, J. Chem. Eng. Data **11** (1966).

[4] S. Akhtar, A. N. M. O. Faruk, and M. A. Saleh, Phys. Chem. Liq. **39**, 383 (2001).

[5] *Landolt-Bönstein New Series IV/25* (Springer, 2008), chap. Viscosity of the mixture (1)water, (2) formamide.

[6] Y. A. Ganiev and Y. L. Rastorguev, J. Eng. Phys. **15**, 519 (1968).

[7] H. D. Young, *University Physics* (Addison Wesley, 1992), 7th ed.

[8] M. N. Hill, ed., *The Sea* (Wiley, 1962), vol. 1.

[9] A. Tobitani and T. Tanaka, Can. J. Chem. Eng. **65**, 321 (1987).

[10] R. F. Checoni and P. L. O. Volpe, J. Solution Chem. **39**, 259 (2010).